INTERNATIONAL JOURNAL FOR NUMERICAL AND ANALYTICAL METHODS IN GEOMECHANICS
Int. J. Numer. Anal. Meth. Geomech. 2015; **39**:988–1013
Published online 3 February 2015 in Wiley Online Library (wileyonlinelibrary.com). DOI: 10.1002/nag.2354

An anisotropic elastic-decohesive constitutive relation for sea ice

Han D. Tran[1,*,†], Deborah L. Sulsky[2,3] and Howard L. Schreyer[3]

[1]*Department of Computational Engineering, Vietnamese-German University, Binh Duong, Vietnam*
[2]*Department of Mathematics and Statistics, The University of New Mexico, Albuquerque, NM 87131, U.S.A.*
[3]*Department of Mechanical Engineering, The University of New Mexico, Albuquerque, NM 87131, U.S.A.*

SUMMARY

Thermodynamic growth or melt and mechanical redistribution due to lead opening or ridge formation shape the thickness distribution of the Arctic ice cover and impact the overall strength of pack ice. Specifically, the deformation and strength of ice are not isotropic but vary with the thickness and lead orientation. To reflect these facts, we develop an anisotropic, elastic-decohesive constitutive model for sea ice together with a model to describe an oriented, ice thickness distribution. The tight connection between the mechanical response and the thickness distribution is an improvement over a previous model that only depended on the average ice thickness. The model describes mechanical responses anisotropically in both the elastic and failure regimes. In the elastic regime, the constitutive relation implicitly reflects strong and weak directions of the pack ice depending on the distribution of thin ice (including open water) and thicker ice (e.g., multi-year ice or ridges). In the failure regime, the model predicts both failure initiation and the lead orientation. Evolution from initial failure to complete failure when traction-free crack surfaces are formed is also modeled. Crack or lead width is determined during the evolution. Various examples of failure surfaces are presented to describe the behavior of modeled ice when the thickness distribution varies. The model predictions are also illustrated and compared with previous modeling efforts by examining regions of ice under idealized loading. Copyright © 2015 John Wiley & Sons, Ltd.

Received 12 August 2014; Revised 16 December 2014; Accepted 23 December 2014

KEY WORDS: sea ice; thickness distribution; decohesion; anisotropic constitutive relation

1. INTRODUCTION

As an interface between the ocean and the atmosphere in polar regions, sea ice plays a significant role in the Earth's thermohaline balance and is an important component of global climate and circulation simulations. The relative movement of pack ice is driven by external forces (i.e., wind, ocean current, sea-surface tilt, and Coriolis forces) and can induce very large internal stresses, and consequently may lead to fractures (i.e., leads or open water) that can extend for thousands of kilometers. In the winter, open water freezes rapidly when exposed to the colder atmosphere. The freezing and melting of ice is governed by thermodynamics. The combined effect of mechanics and thermodynamics results in a range of ice thicknesses, typically described by a thickness distribution function [1, 2]. Moreover, mechanical and thermodynamic processes each depend on the ice thickness, which results in coupling between the processes. Therefore, an accurate simulation of sea ice must account for both mechanics and thermodynamics and their dependence on thickness.

On a small scale, the mechanics of sea ice itself can often be modeled well, up to failure, as an isotropic elastic material characterized by two material constants, which are Young's modulus, E, and Poisson's ratio, ν [3]. However, across the polar regions, sea ice is not a homogeneous

*Correspondence to: Han D. Tran, Department of Computational Engineering, Vietnamese-German University, Binh Duong, Vietnam.
†E-mail: han.td@vgu.edu.vn

medium because of the existence of leads and pressure ridges [1], as well as other flaws. To represent the ice-lead-ridge composite as a continuum, including its failure, Coon *et al.*, [4] proposed a two-dimensional isotropic, elastic-plastic solid model with an associated flow rule. The model was designed to be useful in a numerical simulation using a grid length scale on the order of 100 km where many leads would be present within a computational element. Another constitutive model, introduced by Hibler [5], assumed that pack ice is a viscous-plastic isotropic material that offers strength in compression and shearing but no resistance to tension. Hibler's model and its variations (e.g., [6–9]) have been utilized in practically every global climate model. These types of models do not provide an explicit representation of leads. To overcome this limitation, Schreyer *et al.*, [10] and Sulsky and Peterson [11] proposed an elastic-decohesive model for modeling the dynamics of sea ice. In this model, sea ice deforms elastically and isotropically until the internal stresses reach critical values (determined by a 'decohesion' function) where the initial failure occurs. The decohesion function also determines the orientation of the lead. After the initiation of a crack, further evolution is governed by associated flow rules based on the decohesion function. The advantage of this model is that leads, if any, can be represented explicitly as macrocracks whose orientations and openings are determined via the decohesion function and evolution equations. After failure initiation, the overall mechanical behavior in the model is anisotropic, with material weaker in tensile strength across the fracture, yet retaining its strength along the fracture.

Other anisotropic models have been developed that account for the orientation-dependent weakness in ice due to leads. For example, Hibler and Schulson [12] apply traction continuity on the interface between thick ice and thin, lead ice, together with the assumption of equal strain in the lead direction. In this model, sea ice is assumed to be a viscous-plastic material, and the stress–strain relation is a system of nonlinear equations. Wilchinsky and Feltham [13] use the viscous-plastic rheology and a relation between local and global strain rates so that mean stress can be used, making the model more tractable numerically. An extension of this work in [14] considers sea ice as a layer of granulated thick ice that consists of many rigid brittle floes intersecting along long narrow regions of thinner ice. To avoid the detailed modeling of the fracture process, [15, 16] treat the ice cover as a collection of diamond-shaped flows providing anisotropy through slip lines on diamond boundaries. On the other hand, Weiss *et al.*, [17] develop a damage model, called an elasto-brittle rheology for sea ice, that degrades the Young's modulus, reducing all stress components as the ice weakens.

This paper continues the development of the elastic-decohesive constitutive model [10] with the goal of better connecting the thickness distribution to the stiffness and strength of the pack ice. We should acknowledge that many aspects of this paper have been influenced by the ideas presented in Coon *et al.*, [18]. The basic formulations associated with an elastic-plastic continuum versus failure predicted by an elastic-decohesive discrete constitutive equation are fundamentally different. Nevertheless, the ideas presented by Coon *et al.*, in describing a perfectly plastic yield surface represent insight that is a direct precursor to the current model. Their interpretation of the yield surface as a failure surface with both an isotropic form and an anisotropic form connected to an oriented ice thickness distribution bears considerable similarity to some of the ideas developed in this paper. The failure curves in this work contain many of the attributes outlined in [18].

As noted earlier, the mechanics and thermodynamics of ice affect the thickness, and the thickness, in turn, determines mechanical and thermodynamic properties. In this work, as in our previous work [11], thermodynamic changes to the thickness distribution due to melting and freezing are modeled for a column of ice using the model in [19]. The creation of open water depends on the divergence of the pack due to lead opening and ridges form due to the convergence of the pack, or lead closing. The ridging model described in Lipscomb and Hunke [20, 21] completes the model for the time evolution of the thickness distribution due to mechanics. In the other direction, thickness of pack ice affects the distribution of internal stress. As a simple example, under the same loading conditions, new thin ice can be broken more easily than multiyear thicker ice. The elastic-decohesive model [10, 11] gives the stress per unit thickness of ice, and in these references, the stress resultant is formed by multiplying the stress per unit thickness by the average thickness as determined from the thickness distribution. In the present work, we use the detailed thickness distribution to more tightly couple the mechanical behavior of ice to the thickness. There is no information about the spatial arrangement of the ice within the thickness distribution; however, we make the assumption

DOI: 10.1002/nag

that the thinnest part of the distribution is associated with a lead and is oriented with the lead. This assumption assigns an orientation to the thickness distribution that is tied to the ice mechanics. With this assumption, the stress–strain relation of an ice element is anisotropic both in the elastic and failure regimes. Two elements with the same average thickness, one with constant thickness and the other with a distribution of thicknesses including thin ice, should not deform the same way. Intuitively, the presence of thin ice, especially in a lead, should allow the element to deform more readily in certain directions.

In order to reflect this intuition, we first develop an anisotropic elastic constitutive relation for sea ice having an oriented thickness distribution. The anisotropy develops solely from the thickness distribution. The elastic constants of the anisotropic material are derived using a rule-of-mixtures model that is commonly used in the theory of composites (e.g., [22, 23]). The composite in this case is ice with different thicknesses where a segment of ice with uniform thickness is assumed to deform isotropically. A computational element consisting of different ice thicknesses is replaced by an equivalent homogeneous element of a uniform thickness, but consisting of an anisotropic material. The replacement ensures conservation of volume and strain energy between the original element and the equivalent element. As in previous work, ice deforms elastically until initial failure occurs, where failure is defined by the stress reaching a critical state based on a decohesion function, which depends on the traction and ice strength. This function is an extension of the isotropic version developed by Schreyer *et al.*, [10] because the ice strength now depends on the ice thickness distribution, and therefore on the lead orientation. The evolution of failure with an associated flow rule for the extended model is also addressed in this work.

The paper is organized as follows. In the next section, we summarize the equations that govern the dynamics of sea ice. Although these equations appear elsewhere in the literature, we give them here to define consistent notation for the rest of the paper and to provide a foundation for the discussion of model improvements in the subsequent sections. Section 3 presents the rule-of-mixtures model for the composite, anisotropic elastic moduli. Then, Section 4 describes the failure modeling, specifically by defining the anisotropic ice strengths used in the decohesion function. Evolution of failure is discussed in Section 5. Section 6 examines the behavior of the model under idealized loading conditions such as uniaxial tension and simple shear. These examples show how accounting more precisely for thin ice alters the model predictions compared with relying solely on average thickness. Concluding remarks are made in Section 7.

2. GOVERNING EQUATIONS FOR SEA ICE DYNAMICS

Sea ice mechanics is governed by the momentum balance equation. Because sea ice is thin relative to its extent, the momentum balance is reduced to two dimensions. Variable ice thickness is accounted for through an evolution equation for the ice thickness distribution. Thermodynamics is governed by a heat equation. Heat transfer is only computed in the vertical direction with boundary conditions given by conditions at the atmosphere-ice and ocean-ice surfaces. The momentum equation involves a constitutive relation specifying the stress–strain relation describing ice rheology. Because a constitutive relation for sea ice coupled to the thickness distribution is the key development of the present work, in this section, we first summarize the momentum equation written in terms of 2D quantities and then summarize the governing equation for the thickness distribution. We end this summary by specifying the need for a constitutive relation that can take into account the thickness distribution.

2.1. Momentum equations

A detailed derivation of the reduction from three dimensions to the two-dimensional description of momentum balance, along with the required assumptions, can be found in Gray and Moreland [24]. In this section, we summarize the equations in order to emphasize the connection to the thickness distribution.

Momentum balance is written with respect to a Cartesian right-handed, coordinate system with its origin fixed on the Earth's surface. The in-plane coordinates $\boldsymbol{x} = (x_1, x_2)$ are in a horizontal tangent plane, and the x_3 direction is the vertical direction, normal to the geopotential mean sea

DOI: 10.1002/nag

surface. Curvature is neglected. The velocity, with components $\mathbf{v} = (v_1, v_2)$, is assumed to lie in the 1-2 plane with no out of plane component. The momentum equation in the 1-2 plane can be written

$$m\frac{dv_\alpha}{dt} = \frac{\partial}{\partial x_\beta}\left(N_{\alpha\beta}\right) + \tau_\alpha^a + \tau_\alpha^w + 2m\Omega\sin\phi\epsilon_{\alpha\beta 3}v_\beta - m\hat{g}\frac{\partial z_w}{\partial x_\alpha}, \tag{1}$$

with the indices α and β ranging from 1 to 2 and with repeated indices summed. The quantity m is the mass per unit area of ice. The first term on the right-hand side represents the internal ice forces. The 'extra' stress resultant, $N_{\alpha\beta}$, is a second rank tensor, and it is the difference between the vertically integrated stress in the ice and the vertically integrated hydrostatic load. This extra stress resultant has dimensions of force per unit length and is called extra stress because it is the stress extra to the intrinsic water pressure. The second and third terms are the components of air stress, $\boldsymbol{\tau}^a = \left(\tau_1^a, \tau_2^a\right)$, and water stress, $\boldsymbol{\tau}^w = \left(\tau_1^w, \tau_2^w\right)$, on the ice layer, that are caused by surface winds and ocean currents, respectively. The exact specification of these terms is not needed for this work. The third term is the Coriolis force where Ω is the angular velocity of the Earth about its north-south axis, and ϕ is the latitude of the point $\boldsymbol{x}$. Also in the third term, $\epsilon_{\alpha\beta 3}$ denotes the alternating symbol (i.e., $\epsilon_{123} = -\epsilon_{213} = 1$; $\epsilon_{113} = \epsilon_{223} = 0$). The last term is the acceleration due to the tilting of the sea surface with the acceleration due to gravity denoted by $\hat{g}$ and $z_w(\boldsymbol{x}, t)$ giving the height of the sea surface at the point $\boldsymbol{x}$ at time t [24].

2.2. *Thickness distribution*

The best resolved regional simulations today use a computational element on the order of 1-5 square kilometers. An element of this size can contain ice of varying thickness, from zero thickness (open water), to new ice only centimeters thick, to ridged ice that can be tens of meters thick. The variation of thickness in a given element is incorporated in simulations through a subgrid scale thickness distribution [1, 4]. For a region of ice with area $A(\boldsymbol{x}, t)$, the thickness distribution, $g(\boldsymbol{x}, h, t)$, is defined such that

$$\int_{h_i}^{h_{i+1}} g(\boldsymbol{x}, h, t)\, dh = \frac{A_i(\boldsymbol{x}, t)}{A(\boldsymbol{x}, t)} \tag{2}$$

where A_i is the area within this region that is covered by ice of thickness h in the range $h_i \leq h < h_{i+1}$. The function g is analogous to a probability distribution and when integrated over thickness space ($h \in [0, \infty)$) is equal to one. Note that for the special case where the element contains only open water, the function g is a Dirac delta function at $h = 0$. The governing equation for the thickness distribution is expressed as follows [1]

$$\frac{\partial g}{\partial t} = -\frac{\partial}{\partial x_\alpha}(v_\alpha g) - \frac{\partial}{\partial h}(fg) + \psi. \tag{3}$$

The function $f(h) = dh/dt$ is the thermodynamic growth rate, and ψ is a function describing the mechanical redistribution of ice accounting for ridge formation in converging flow or the creation of open water in diverging flow. The thermodynamic growth rate is determined by solving a heat equation through the ice thickness. A detailed specification of f and ψ are not needed for this work, but can be found in [11], which in turn is based on [21] and [25].

The thickness distribution can be used to define effective or mean properties of the ice cover over the area A. For example, the mass per unit area, m, equals

$$m(\boldsymbol{x}, t) = \int_0^\infty \rho_{\text{ice}} h g(\boldsymbol{x}, h, t)\, dh, \tag{4}$$

where ρ_{ice} is the density of ice. It is reasonable to consider ρ_{ice} to be constant, and then $m = \rho_{\text{ice}}\overline{h}$ where $\overline{h}(\boldsymbol{x}, t) = \int_0^\infty hg(\boldsymbol{x}, h, t)\ dh$ is the mean ice thickness. This relationship is the first connection between the thickness distribution and the momentum equation describing ice dynamics

DOI: 10.1002/nag

because m appears in Equation (1). The goal of this paper is to examine the role of the thickness distribution, described by the function $g(\boldsymbol{x}, h, t)$ in determining the extra stress resultant $\mathbf{N}(\boldsymbol{x}, t)$. To this end, we will examine how the extra stress *per unit thickness* of ice, $\boldsymbol{\sigma}(\boldsymbol{x}, t)$, is related to the stress resultant, $\mathbf{N}$, through the thickness distribution. Note that $\boldsymbol{\sigma}$ has dimensions of force per unit area and is physically stress. Being the stress resultant, $\mathbf{N}$ has units of force per unit length.

The relationship between the stress and the stress resultant is [4]

$$\mathbf{N}(\boldsymbol{x}, t) = \frac{1}{A} \int_A \left(\int_0^{\zeta} \boldsymbol{\sigma} \, dx_3 \right) da \tag{5}$$

where $\zeta(\boldsymbol{x}, t)$ is the ice thickness at $\boldsymbol{x} \in A$. If the stress $\boldsymbol{\sigma}$ is constant through the thickness, that is, does not depend on x_3, then

$$\mathbf{N}(\boldsymbol{x}, t) = \frac{1}{A} \int_A \zeta \boldsymbol{\sigma} \, da. \tag{6}$$

The area integral can be converted to an integral over h using the thickness distribution in A. If the stress $\boldsymbol{\sigma}$ depends on the ice thickness, $\boldsymbol{\sigma} = \hat{\boldsymbol{\sigma}}(\boldsymbol{x}, h, t)$, then

$$\mathbf{N}(\boldsymbol{x}, t) = \int_0^{\infty} h \hat{\boldsymbol{\sigma}}(\boldsymbol{x}, h, t) g(\boldsymbol{x}, h, t) \, dh. \tag{7}$$

Finally, note that if $\boldsymbol{\sigma}$ does not depend on h, then $\mathbf{N} = \overline{h}\boldsymbol{\sigma}$. In fact, it is this expression for $\mathbf{N}$ that was used in previous work (e.g., [26]). In this paper, we argue that the stress $\boldsymbol{\sigma}$ (and the strain) can depend on h, and we incorporate this dependence into the constitutive relation for $\mathbf{N}$ when it occurs.

In the next section, we derive the thickness-dependent constitutive model for $\mathbf{N}$ in the elastic regime, and then in the following section, we examine the failure regime. When an element of ice has failed and there is a modeled orientation to that failure or lead, we assume that $g(\boldsymbol{x}, h, t)$ is oriented with the lead, and the thinnest ice is in the lead. In this paper, we use the term 'lead' broadly, as in [18], to mean not only an area of open water due to a fracture in the ice but also to describe long narrow features that contain new ice, ruble ice, or a previous fracture that has not yet regained the strength of intact ice. This orientation of the thickness introduces anisotropy into the constitutive model, even in the elastic regime. If there is no lead predicted in the element, then we revert to using the average thickness, isotropic elasticity, and our original decohesive model. A more detailed description of an oriented thickness distribution is possible [18, 27] in which a separate distribution is used for lead ice and intact ice with rules for transitioning between the two. While not as detailed, the assumption that the thinnest part of a single distribution g can be associated with the ice in the lead simplifies the computations and appears to suffice.

3. DERIVATION OF ELASTIC CONSTANTS OF THE EQUIVALENT SYSTEM

The aim of this analysis is to ask what the effective, or equivalent, properties of an element of ice of area A should be in order to capture information about the deformation of ice within that area when the ice has variable thickness. We assume that on a small scale, the ice is homogeneous and isotropic, characterized by known values of E and ν. We determine the aggregate response of this ice on a large scale due to the distribution of thicknesses within the aggregate. The essential concept is analogous to determining the effective stiffness of a device consisting of two springs. The effective stiffness depends on whether the springs are arranged in parallel or in series. In series, the elongations for the two springs add, but they each have the same force, resulting in an effective stiffness that is the harmonic mean of the two stiffnesses. In parallel, the two springs have the same elongation and the forces add, resulting in an effective stiffness that is the arithmetic mean of the two

DOI: 10.1002/nag

stiffnesses. In the case of ice, ice with differing thickness has differing stiffness. Thus, a 'parallel' or 'series' arrangement of thickness with respect to the loading direction yields a different response.

In computational implementations, the thickness space is discretized into a finite number of categories on which the function g is approximated (e.g., [28]). Each category has an average thickness h_i and a fractional area a_i, where $i = [1, N]$ and N is the number of categories. It is easiest to illustrate the model in this discrete setting, and we start the derivation by examining two categories, $N = 2$. For simplicity, consider the case of a square unit element that contains two thickness categories as shown in Figure 1(a). The extension to the multi-category case is straightforward and will be discussed at the end of this section. The thickness and length of the categories are $\{h_1, l_1\}$ and $\{h_2, l_2\}$, respectively. Both categories have the same width, $w = l_1 + l_2$. The objective here is to replace the original element, Figure 1(a), by an equivalent element of the same area, with a uniform thickness, h_p, so that the effective stress resultant is the thickness of the equivalent element times the effective stress, $\mathbf{N} = h_p\boldsymbol{\sigma}$, as shown in Figure 1(b). The replacement is based on the requirement that under the same loading, the overall deformation of the two elements should be the same so that the strain energy is conserved. The thickness of the equivalent element, denoted by h_p (p for parallel), is based on conservation of volume and is

$$h_p(l_1 + l_2)w = h_1 l_1 w + h_2 l_2 w \rightarrow h_p = \frac{h_1 l_1 w + h_2 l_2 w}{w(l_1 + l_2)} = a_1 h_1 + a_2 h_2. \tag{8}$$

All of the results that follow in this section are derived with respect to a Cartesian coordinate system defined such that the 1 and 2 directions are perpendicular and parallel, respectively, to the geometric arrangement of the categories, as shown in Figure 1(a). These directions are called principal material directions because their definition is based on the orientation of the categories. More generally, the 1 direction is perpendicular to the lead direction, and the 2 direction is parallel to the lead direction, and the thickness distribution is aligned so that the thin ice is in the lead. The effective material properties of the equivalent element are anisotropic and consist of the moduli E_i, shear moduli G_{ij}, and Poisson's ratios ν_{ij}, with $i, j \in \{1, 2\}$ and $i \neq j$, and are derived using a rule-of-mixtures model as shown in the succeeding text.

3.1. Model for E_1

Assume as in Figure 2(a) that the original element is subjected to a stress resultant F_{11} such that the element elongates in the 1 direction (and contracts in the 2 direction due to Poisson effects). Under this loading, the normal stress in the 1 direction of each category is

$$\sigma_{11}^{(1)} = \frac{F_{11}}{wh_1} \quad \text{and} \quad \sigma_{11}^{(2)} = \frac{F_{11}}{wh_2}, \tag{9}$$

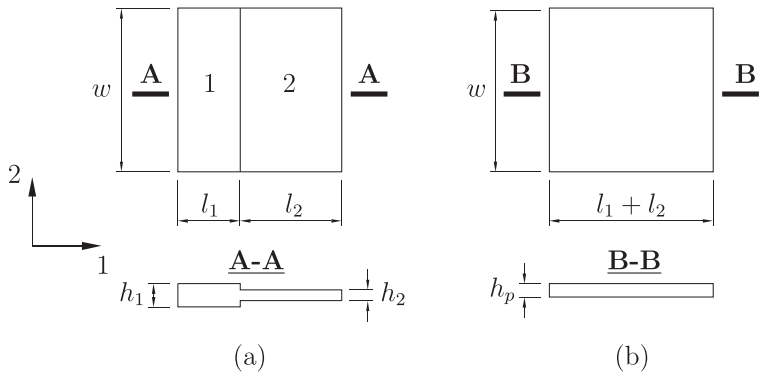

Figure 1. (a) Original element with two categories of different thicknesses; (b) equivalent element of a uniform thickness and the same area as the original one.

DOI: 10.1002/nag

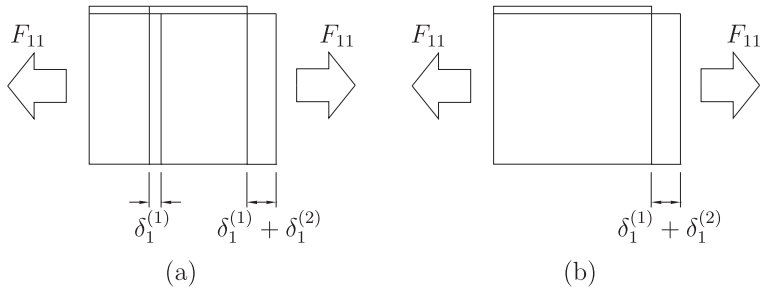

Figure 2. (a) Deformation of the original element under uniaxial loading in the 1 direction; (b) deformation of the equivalent element under the same loading.

in which the superscript on σ refers to the category number. With the assumption that there is only normal stress in the 1 direction generated in both categories, the strain in the 1 direction for each category is

$$\varepsilon_{11}^{(1)} = \frac{\sigma_{11}^{(1)}}{E} \qquad \text{and} \qquad \varepsilon_{11}^{(2)} = \frac{\sigma_{11}^{(2)}}{E}, \tag{10}$$

where E is the Young's modulus of homogenous ice on the small scale. If we denote $\delta_1^{(1)}$ and $\delta_1^{(2)}$ as the elongations of categories 1 and 2, respectively, as shown in Figure 2(a), then we have the following relation

$$\delta_1^{(1)} = l_1 \varepsilon_{11}^{(1)} \qquad \text{and} \qquad \delta_1^{(2)} = l_2 \varepsilon_{11}^{(2)}. \tag{11}$$

The combination of (9), (10), and (11) results in

$$\delta_1^{(1)} + \delta_1^{(2)} = \frac{F_{11}}{Ew}\left(\frac{l_1}{h_1} + \frac{l_2}{h_2}\right). \tag{12}$$

Under the same application of the stress resultant, F_{11}, as with springs in series, the equivalent element has to elongate an amount of $\delta_1^{(1)} + \delta_1^{(2)}$ as shown in Figure 2(b). Thus, the normal stress and strain in the 1 direction of the equivalent element is

$$\sigma_{11} = \frac{F_{11}}{wh_p} \qquad \text{and} \qquad \varepsilon_{11} = \frac{\delta_1^{(1)} + \delta_1^{(2)}}{l_1 + l_2}. \tag{13}$$

Because there is no normal stress in the 2 direction and no shear stress, the extensional modulus in the 1 direction of the equivalent material is $E_1 = \sigma_{11}/\varepsilon_{11}$. Therefore, from (12) and (13), we obtain the result

$$E_1 = \frac{h_1 h_2 (l_1 + l_2)}{h_p (h_1 l_2 + h_2 l_1)} E = \frac{h_1 h_2}{h_p (a_2 h_1 + a_1 h_2)} E. \tag{14}$$

A thickness h_s (s for series) is defined as

$$\frac{1}{h_s} = \frac{a_1}{h_1} + \frac{a_2}{h_2}. \tag{15}$$

Then Equation (14) can be written in a contracted form as

$$E_1 = \frac{h_s}{h_p} E. \tag{16}$$

DOI: 10.1002/nag

As can be seen in (14), the value of E_1 goes to zero when one of the categories has zero thickness (i.e., the ice in this category melts completely). This observation means that the equivalent element does not have load-carrying capacity in the 1 direction when one category is open water. This feature enables our developed constitutive relation to represent implicitly open water in the thickness distribution. It is also noted that

$$h_p - h_s = \frac{(h_1 - h_2)^2 a_1 a_2}{(a_1 h_2 + a_2 h_1)} \geq 0 \tag{17}$$

for any non-negative values of thickness h_i and area fractions a_i, $i \in \{1, 2\}$. This observation means that E_1 is always smaller than or equal to E.

3.2. *Model for* E_2

Assume as in Figure 3(a) that the original element is subjected to a stress resultant F_{22} such that the element elongates in the 2 direction (and contracts in the 1 direction due to Poisson effects). The normal stress in the 2 direction of the categories is related to the stress resultant by

$$\sigma_{22}^{(1)} h_1 l_1 + \sigma_{22}^{(2)} h_2 l_2 = F_{22}. \tag{18}$$

With the assumption that there is only normal stress in the 2 direction in both categories, the strain in the 2 direction for each category is

$$\varepsilon_{22}^{(1)} = \frac{\sigma_{22}^{(1)}}{E} \qquad \text{and} \qquad \varepsilon_{22}^{(2)} = \frac{\sigma_{22}^{(2)}}{E}. \tag{19}$$

Because the categories are 'bonded' together, as with springs in parallel, they both elongate the same amount in the 2 direction, namely, δ_2 as shown in Figure 3(a). We then have the following relation

$$\delta_2 = w\varepsilon_{22}^{(1)} = w\varepsilon_{22}^{(2)}. \tag{20}$$

Under the same application of the stress resultant, F_{22}, the equivalent element has to elongate an amount of δ_2 as shown in Figure 3(b). Thus, the normal stress and strain in the 2 direction for the equivalent element is

$$\sigma_{22} = \frac{F_{22}}{h_p(l_1 + l_2)} \qquad \text{and} \qquad \varepsilon_{22} = \frac{\delta_2}{w}. \tag{21}$$

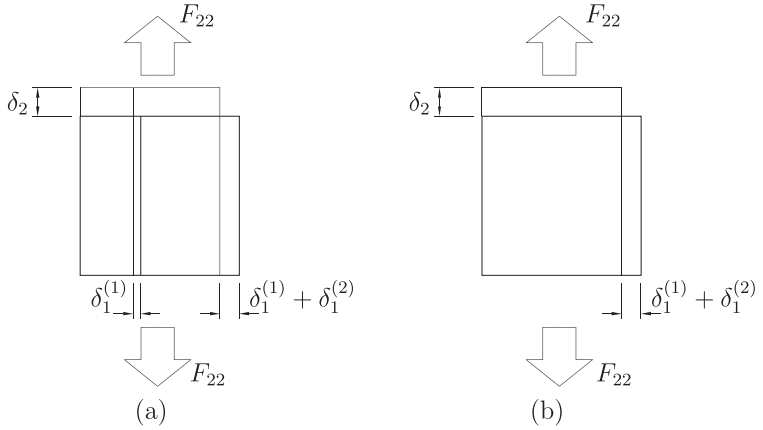

Figure 3. (a) Deformation of the original element under uniaxial loading in the 2 direction; (b) deformation of the equivalent element under the same loading.

DOI: 10.1002/nag

Combining (18), (19), and (20) and the second part of (21), we have

$$\varepsilon_{22} = \frac{F_{22}}{E(h_1 l_1 + h_2 l_2)}. \tag{22}$$

Because there is no normal stress in the 1 direction and no shear stress, the extensional modulus in the 2 direction of the equivalent material is $E_2 = \sigma_{22}/\varepsilon_{22}$. Therefore, with the use of the first part of (21) and (22), we obtain the result

$$E_2 = \frac{E(h_1 l_1 + h_2 l_2)}{h_p(l_1 + l_2)} = \frac{E(a_1 h_1 + a_2 h_2)}{h_p}. \tag{23}$$

Recalling the definition of h_p given in (8), the final result is

$$E_2 = E. \tag{24}$$

Regardless of the thickness distribution, the value of E_2 is always a constant that is the Young's modulus of the original material. As shown in the previous section, we have $E_1 \leq E$. Therefore, the 1 direction always has less or equal stiffness than the 2 direction of the equivalent element.

3.3. Model for ν_{21}

Assume again that the original element is subjected to a stress resultant F_{22} as shown in Figure 3(a). Because both categories have the same Poisson's ratio ν, their strains in the 1 direction are the same

$$\varepsilon_{11}^{(1)} = \varepsilon_{11}^{(2)} = -\nu \frac{\delta_2}{w}. \tag{25}$$

Denote $\delta_1^{(1)}$ and $\delta_1^{(2)}$ the shrinkages of each category in the 1 direction, as shown in Figure 3(a). Then, we have the following result

$$\delta_1^{(1)} = l_1 \left|\varepsilon_{11}^{(1)}\right| = l_1 \nu \frac{\delta_2}{w} \qquad \text{and} \qquad \delta_1^{(2)} = l_2 \left|\varepsilon_{11}^{(2)}\right| = l_2 \nu \frac{\delta_2}{w}, \tag{26}$$

in which the absolute value is used because the strain in the 1 direction under the application of F_{22} is commonly negative. The shrinkage of the equivalent element is $\delta_1^{(1)} + \delta_1^{(2)}$ as shown in Figure 3(b). Thus, the strain in the 1 direction of the equivalent element is

$$|\varepsilon_{11}| = \frac{\delta_1^{(1)} + \delta_1^{(2)}}{l_1 + l_2}. \tag{27}$$

Using the result (26), with the note that $\varepsilon_{11} < 0$, we have

$$\varepsilon_{11} = -\nu \frac{\delta_2}{w}. \tag{28}$$

The combination of (21) and (28) results in

$$\varepsilon_{11} = -\nu \varepsilon_{22}. \tag{29}$$

By definition of the Poisson's ratio ν_{21}, we have the final result

$$\nu_{21} = \nu. \tag{30}$$

The value of Poisson's ratio ν_{12} is deduced from the symmetry of the compliance matrix, that is, $\nu_{12}/E_1 = \nu_{21}/E_2$.

DOI: 10.1002/nag

3.4. Model for G_{12}

Assume the original element is under pure shear loading with the stress resultant F_{12} and F_{21} as shown in Figure 4. Because the element is square, $F_{12} = F_{21}$ due to moment equilibrium. Under this loading, the shear stress in each category is

$$\tau_{12}^{(1)} = \frac{F_{12}}{wh_1} \qquad \text{and} \qquad \tau_{12}^{(2)} = \frac{F_{12}}{wh_2}. \tag{31}$$

With the assumption that there is only shear stress generated in both categories, the (engineering) shear strains in each category are

$$\gamma_{12}^{(1)} = \frac{\tau_{12}^{(1)}}{G} \qquad \text{and} \qquad \gamma_{12}^{(2)} = \frac{\tau_{12}^{(2)}}{G}, \tag{32}$$

where G is the shear modulus of the original material, that is, $G = E/(2 + 2\nu)$. Denote by $\delta_2^{(1)}$ and $\delta_2^{(2)}$, the shear displacement in the 2 direction for each category, and by δ_1 the shear displacement in the 1 direction of both categories as shown in Figure 4(a). Then, we have the following relations

$$\gamma_{12}^{(1)} = \frac{\delta_1}{w} + \frac{\delta_2^{(1)}}{l_1} \qquad \text{and} \qquad \gamma_{12}^{(2)} = \frac{\delta_1}{w} + \frac{\delta_2^{(2)}}{l_2}. \tag{33}$$

In (33), we multiply the first part with l_1 and the second part with l_2, then add them together to have the following relation to be used in a later calculation of the shear strain of the equivalent element

$$l_1\gamma_{12}^{(1)} + l_2\gamma_{12}^{(2)} = \frac{\delta_1}{w}(l_1 + l_2) + \delta_2^{(1)} + \delta_2^{(2)}. \tag{34}$$

Under the same loading, the equivalent element has to deform as indicated in Figure 4(b). Thus, the shear stress and shear strain are

$$\tau_{12} = \frac{F_{12}}{wh_p} \qquad \text{and} \qquad \gamma_{12} = \frac{\delta_1}{w} + \frac{\delta_2^{(1)} + \delta_2^{(2)}}{l_1 + l_2}. \tag{35}$$

Using (34), we can re-write the second part of (35) as

$$\gamma_{12} = \frac{l_1\gamma_{12}^{(1)} + l_2\gamma_{12}^{(2)}}{l_1 + l_2}. \tag{36}$$

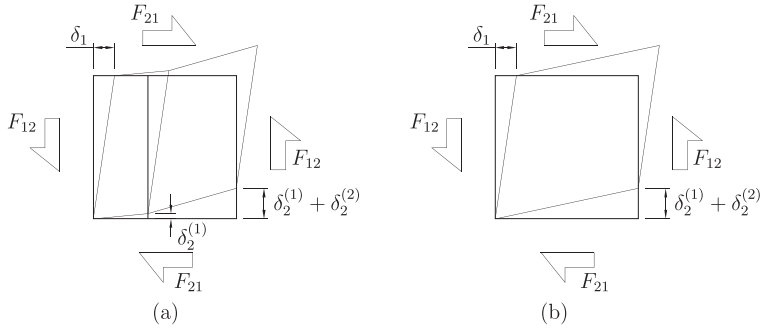

Figure 4. (a) Deformation of the original element under pure shear loading; (b) deformation of the equivalent element under the same shear loading.

DOI: 10.1002/nag

Continuing, using (31) and (32), we have

$$\gamma_{12} = \frac{l_1 \frac{F_{12}}{Gwh_1} + l_2 \frac{F_{12}}{Gwh_2}}{l_1 + l_2}. \tag{37}$$

The shear modulus of the equivalent material is computed as $G_{12} = \tau_{12}/\gamma_{12}$. Using the first part of (35) and (37), we obtain the result

$$G_{12} = \frac{h_1 h_2 (l_1 + l_2)}{h_p (h_2 l_1 + h_1 l_2)} G = \frac{h_1 h_2}{h_p (a_1 h_2 + a_2 h_1)} G. \tag{38}$$

With the definition of h_s in (15), the shear modulus, G_{12}, is written more compactly as

$$G_{12} = \frac{h_s}{h_p} G. \tag{39}$$

Similar to E_1, the shear modulus G_{12} goes to zero (i.e., the material does not offer any shear stiffness) when one of the categories has zero thickness, and also G_{12} is always smaller than or equal to G.

3.5. Summary of the elastic constants and extension to the multi-category case

The elastic constants of the anisotropic material of the equivalent element shown in Figure 1(b) can be summarized in the following stress strain relation

$$\begin{bmatrix} \varepsilon_{11} \\ \varepsilon_{22} \\ \gamma_{12} \end{bmatrix} = \begin{bmatrix} \frac{1}{kE} & \frac{-\nu}{E} & 0 \\ \frac{-\nu}{E} & \frac{1}{E} & 0 \\ 0 & 0 & \frac{1}{kG} \end{bmatrix} \begin{bmatrix} \sigma_{11} \\ \sigma_{22} \\ \tau_{12} \end{bmatrix}, \qquad k = h_s/h_p. \tag{40}$$

This matrix form summarizes the relations given in (16), (24), (29), (30), and (39). The parameter k is an anisotropy factor that indicates the difference between the extensional modulus E_1 in the 1 direction and the Young's modulus E of the original material, and the difference between the shear modulus G_{12} and shear modulus G of the original material.

Now, consider the case where the original element contains N categories ($N \geq 1$) whose geometries are arranged as shown in Figure 5(a), for the example, when $N = 4$. In this figure,

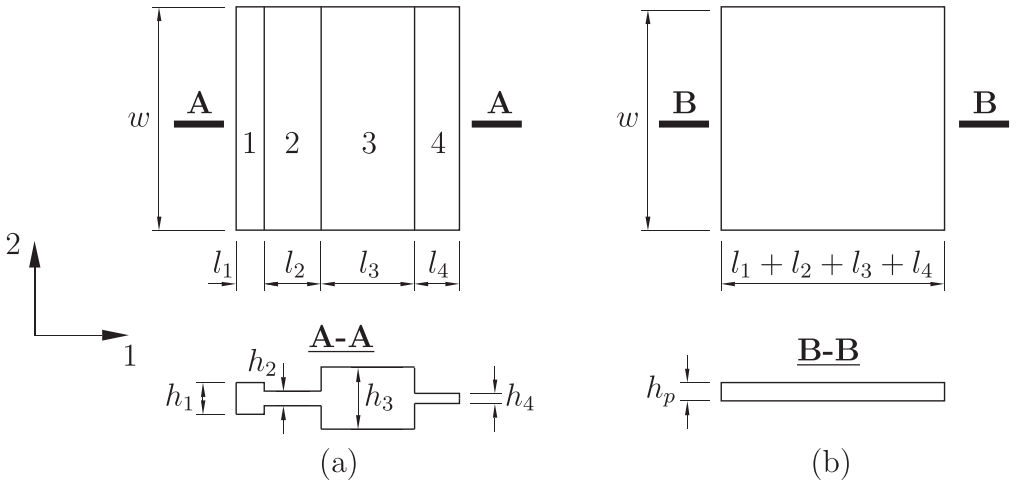

Figure 5. (a) Sketch of the original element with four categories of different thicknesses; (b) the equivalent element of uniform thickness and the same area as the original one.

DOI: 10.1002/nag

$\{h_i, l_i\}, i \in \{1, 2, 3, 4\}$, is the thickness and length of category i. All categories have the same width of $w = l_1 + l_2 + l_3 + l_4$. Again, the objective is to replace the original element by an equivalent element, which has a uniform thickness h_p as shown in Figure 5(b), such that both systems deform equivalently under the same loading. Note that the equivalent element has the same area as the original one, and a thickness of

$$h_p = \frac{\sum_{i=1}^{N} h_i l_i}{\sum_{i=1}^{N} l_i} = \sum_{i=1}^{N} a_i h_i \tag{41}$$

to ensure conservation of volume. The procedure to obtain the elastic constants of the anisotropic material of the equivalent element for the multi-category case follows the same arguments as for the two-category case. The final result is a compliance matrix in the same form as Equation (40), in which h_s is defined as

$$\frac{1}{h_s} = \frac{\sum_{i=1}^{N} (l_i / h_i)}{\sum_{i=1}^{N} l_i} = \sum_{i=1}^{N} \frac{a_i}{h_i}. \tag{42}$$

As before, it can be shown that $h_p \geq h_s$ (i.e., $k \leq 1$), and $h_s = 0$ when one of the categories has zero thickness.

In terms of the continuum formulation of Section 2, we have assumed that the small-scale stress, $\boldsymbol{\sigma} = \hat{\boldsymbol{\sigma}}(\boldsymbol{x}, h, t)$ and the small-scale strain, $\boldsymbol{\varepsilon} = \hat{\boldsymbol{\varepsilon}}(\boldsymbol{x}, h, t)$, are related by a linear, isotropic model in the elastic regime,

$$\hat{\boldsymbol{\sigma}} = \mathbb{C}^{\text{iso}} : \hat{\boldsymbol{\varepsilon}} \tag{43}$$

where $\mathbb{C}^{\text{iso}}$ is a constant, isotropic, fourth-order, elastic, compliance tensor defined by the two elastic parameters, E and ν. On the other hand, the effective elastic properties for the region A were determined to be anisotropic, with corresponding linear elastic, constitutive model

$$\boldsymbol{\sigma} = \mathbb{C} : \boldsymbol{\varepsilon} \tag{44}$$

where $\mathbb{C} = \mathbb{C}(k, \overline{\mathbf{n}})$. The value of $k = h_s / h_p$ is determined from

$$h_p = \int_0^\infty h g(\boldsymbol{x}, h, t)\, dh \tag{45}$$

$$\frac{1}{h_s} = \int_0^\infty \frac{1}{h} g(\boldsymbol{x}, h, t)\, dh \tag{46}$$

and $\overline{\mathbf{n}}$ is a unit normal vector to the lead. A vector, $\overline{\mathbf{t}}$, tangent to the crack surface can be determined from $\overline{\mathbf{n}}$ in the plane of the ice. Together, $\overline{\mathbf{n}}$ and $\overline{\mathbf{t}}$ can be chosen to be basis vectors associated with the material axes used earlier. The components summarized in (40) are the components of the inverse of $\mathbb{C}$ in Voigt notation, given in terms of the material bases determined by $\overline{\mathbf{n}}$.

The stress resultant, $\mathbf{N}$ in (7), is now defined by replacing the local, small-scale stress with the effective stress (44). Because the effective stress does not depend explicitly on h, we have $\mathbf{N} = \overline{h}\boldsymbol{\sigma}$. Notice that the definition of h_p in (46) is the same as the definition of $\overline{h}$ in Section 2. We view h_p as the effective thickness, so we could also define an effective thickness distribution, $\overline{g}(\boldsymbol{x}, h, t) = \delta(h - h_p)$, which gives the same stress resultant, $\mathbf{N} = \overline{h}\boldsymbol{\sigma}$, from (7).

DOI: 10.1002/nag

4. MATERIAL FAILURE

The decohesive failure model developed by Schreyer *et al.*, [10] has two aspects. The first aspect is the development of a failure function that describes a curve in stress space, which determines the stress when failure begins and the orientation of the any potential crack. The second aspect is a model determining how failure evolves once it is predicted to initiate. The first aspect of the decohesive model is examined in this section, and the second aspect is studied in the next section.

In [10], the failure function before failure begins describes an isotropic failure curve. However, if there is ice with varying thickness, we might expect the thinner ice to be more susceptible to failure, depending on how the thin ice is oriented relative to the loading direction. Because the expected behavior of an element of ice with varying thickness depends on the loading direction, the failure curve should be anisotropic. This section presents a criterion that captures information about the thickness variation to predict the failure of an equivalent element of ice of uniform thickness. We begin with a summary of the isotropic model in order to be able to highlight the changes we are proposing. After describing the model, two typical examples of an initial failure curve are used to illustrate the general features of the model. Then, the extension of the model for an anisotropic material is discussed. Lastly, examples of anisotropic initial failure curves for various thickness distributions are presented at the end of the section and compared with the two typical isotropic initial failure curves.

4.1. Summary of the isotropic model

The initial failure under external loading of a material is predicted by a failure function F, which is defined such that [10]

$$F = \max_{\mathbf{n}} F_n(\boldsymbol{\tau}, \sigma_{ss}) \tag{47}$$

where $\boldsymbol{\tau}$ is the traction vector on the plane defined by the unit normal vector $\boldsymbol{n}$, and σ_{ss} is the normal stress component in the tangential direction $\boldsymbol{s}$ of this plane. Note that, unless $\boldsymbol{n}$ is a principal direction, the unit tangent vector $\boldsymbol{s}$ is taken to lie on the projection of the traction $\boldsymbol{\tau}$ onto this plane, that is,

$$\boldsymbol{s} = \frac{\boldsymbol{\tau} - (\boldsymbol{\tau}.\boldsymbol{n})\boldsymbol{n}}{\|\boldsymbol{\tau} - (\boldsymbol{\tau}.\boldsymbol{n})\boldsymbol{n}\|}. \tag{48}$$

The function F_n associated with $\boldsymbol{n}$ is defined as follows

$$F_n = \frac{\tau_s^2}{(s_m \tau_{sf})^2} + \exp\left(\kappa\left(\frac{\tau_n}{\tau_{nf}} + \frac{\langle -\sigma_{tt}\rangle^2}{f_c'^2} - 1\right)\right) - 1 \tag{49}$$

where

$$\langle x \rangle = \begin{cases} x & \text{if } x \geq 0 \\ 0 & \text{if } x < 0 \end{cases},$$

and τ_n and τ_s are the components of the traction $\boldsymbol{\tau}$ in the $\boldsymbol{n}$ and $\boldsymbol{s}$ directions, respectively (i.e., $\tau_n = \boldsymbol{\tau}.\boldsymbol{n}$ and $\tau_s = \boldsymbol{\tau}.\boldsymbol{s}$). The material parameters $\{\tau_{nf}, \tau_{sf}\}$ are defined as the failure stress for pure tension and for pure shear, respectively, and f_c' is the failure stress under uniaxial compression. Also, s_m multiplied by the shear failure, τ_{sf}, is the maximum possible value for the shear failure under large normal compressive stress, and κ is related to s_m through the relation $s_m^2(1 - e^{-\kappa}) = 1$ [10].

Analogous to a yield function in plasticity theory, the value of F indicates the state of material deformation, for example, $F < 0$ is an elastic state, $F = 0$ indicates failure, and $F > 0$ is not allowed. Typically, when ice is loaded, we begin with $F < 0$, which indicates that the constitutive

DOI: 10.1002/nag

behavior is in the elastic regime. Failure initiates when F reaches zero for some value of $\boldsymbol{n}$, and this value of $\boldsymbol{n}$ determines the normal to the physical crack forming in the ice, and thus determines the orientation of a lead. In [10], the search for the maximum value of F_n in (47) is restricted to vectors $\boldsymbol{n}$ in the plane of the ice. In this work, the search is taken over all possible directions of the normal vector $\boldsymbol{n}$ in three-dimensional space. This feature enables the model to predict out-of-plane failure in compressive loading.

For the isotropic failure curve with failure parameters $\left\{\tau_{nf}, \tau_{sf}, f_c^{'}, s_m\right\}$, initial failure under a given loading condition can be predicted using the decohesion function defined in (47) and (49). Figure 6 shows two examples of the initial failure curve. The materials employed in these examples have failure parameters shown in Table I. The failure curve defined by $F = 0$ for each material is plotted in the coordinate system of principal stress directions $\{\boldsymbol{p}_1, \boldsymbol{p}_2\}$ where σ_1 and σ_2 are principal stresses associated with these principal directions. Note that the third principal stress, $\sigma_3 = 0$, is due to the plane stress assumption. Table II shows the direction of the normal vector $\boldsymbol{n}$ in each of the segments of the failure curve, which is partitioned by the vertices $\{a_1, b_1, c_1, d_1\}$ and $\{a_2, b_2, c_2, d_2\}$ as shown in Figure 6(a). Note that a normal $\boldsymbol{n}$ can be parameterized by two spherical coordinates $\{\phi, \theta\}$, as shown in Figure 6(b). Because the failure function F is isotropic, the failure curve and the direction of the normal vector are each symmetric about the plane whose projection onto the $\boldsymbol{p}_1 - \boldsymbol{p}_2$ plane is the bisector of the first quadrant. Therefore, the directions of $\boldsymbol{n}$ are given only on half of each failure curve in Table II.

For the first material, the failure surface is always perpendicular to the maximum principal direction. Especially, for the third quadrant, the normal vector is in the direction of $\boldsymbol{p}_3$ because $\sigma_3 = 0$ is the maximum principal stress when σ_1 and σ_2 are both negative. This mode of failure models crushing of pack ice and its piling up into ridges (and down into keels) under biaxial compressive stresses as illustrated in Figure 7. The second material has a value of the failure stress in pure shear, τ_{sf}, decreased by a factor of three compared with the first material. Its failure curve, shown in Figure 6(a), is smaller than that of the first material. It can be seen that, for this material,

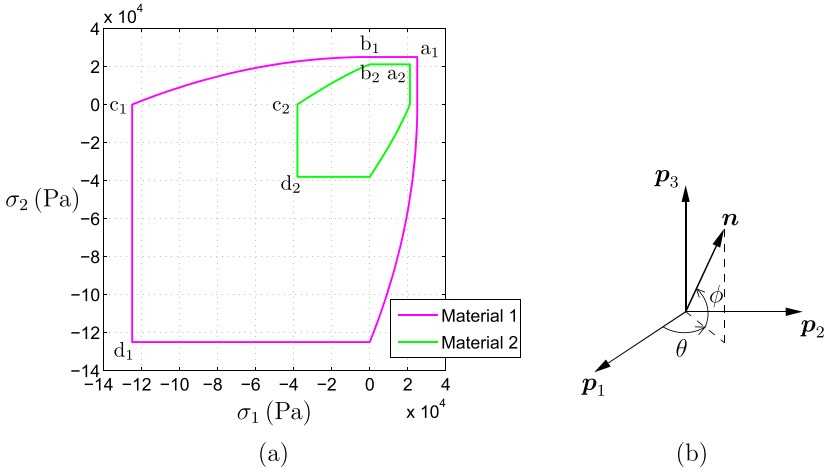

Figure 6. (a) Initial failure curves of the materials whose failure parameters are shown in Table I; (b) definition of the normal vector $\boldsymbol{n}$ to the crack in the coordinate system of principal stress directions.

Table I. Failure parameters of the material whose initial failure curves are shown in Figure 6.

	τ_{nf} (kPa)	τ_{sf} (kPa)	$f_c^{'}$ (kPa)	s_m
Material 1	25	75	125	4
Material 2	25	15	125	4

DOI: 10.1002/nag

Table II. Direction of the normal vector $\boldsymbol{n}$ to the crack, corresponding to the failure curves in Figure 6.

	Material 1		Material 2		
	$a_1 - c_1$	$c_1 - d_1$	$a_2 - b_2$	$b_2 - c_2$	$c_2 - d_2$
ϕ	0^o	90^o	$\pm 32^o$	0^o	$\pm 52^o$
θ	90^o	–	90^o	$\pm 58^o \rightarrow \pm 52^o$	0^o

Figure 7. Illustration of crushing of pack ice under biaxial compressive stresses.

a mixed-mode failure occurs as a result of a combination of normal and shear stress components on the initiating crack. The low value of τ_{sf} relative to τ_{nf} means that neither the tensile failure stress, τ_{nf}, nor the compressive failure stress, f_c', is attained. These values are interpreted as failure values associated with brittle materials, which have a large value of τ_{sf}, as exhibited by material 1. Moreover, for material 2, the normal vector to the crack is not in one of the principal directions but somewhere between them. It is observed that the normal vector to the crack plane for all isotropic materials is always in the plane of maximum and minimum principal directions.

4.2. Failure stresses for an anisotropic material

The decohesion function (49) is now applied to an anisotropic material whose failure stresses $\left\{\tau_{nf}, \tau_{sf}, f_c^{'}\right\}$ are not constants but depend on the crack orientation when there is a varying thickness distribution. We assume that these failure stresses are constant and known on the small scale. Similar to the case of elastic constants, the failure stresses (i.e., strengths) in the direction of material axes are derived using a rule-of-mixtures model. A simple case of two thickness categories is employed for the derivation. The extension to the general case of multiple categories follows. After having the failure stresses in the directions of the material axes, we can obtain the failure stresses in an arbitrary direction by employing an assumed interpolation expression from the three basic corresponding values in the material directions. We remark that, in the derivation of the basic failure stresses, it is assumed that the failure shear stress τ_{sf} is large enough compared with the failure tension stress τ_{nf} (e.g., $\tau_{sf} \geq 3\tau_{nf}$) so that under uniaxial tension or compression, the material fails with a pure mode-I fracture. Schulson's [29] experiments support this assumption for laboratory ice because they indicate that the normal to the failure plane is in the maximum stress direction for the quadrant where one principal stress is positive and the other is negative.

4.2.1. Failure stresses for pure tension. For the failure stress in the 1 direction, assume again that the original element is subjected to a stress resultant F_{11} as shown in Figure 2. Suppose $h_2 \leq h_1$, which results in $\sigma_{11}^{(2)} \geq \sigma_{11}^{(1)}$. Thus, category 2 will fail first once its stress reaches the failure stress in tension of the material, that is, $\sigma_{11}^{(2)} = \tau_{nf}$. Note that the failure of category 2 makes the whole system fail under tension, and the failure stress resultant is

$$F_{11}^{cr} = \tau_{nf} h_2 w. \tag{50}$$

Therefore, the failure stress for pure tension of the equivalent element will be

$$\tau_{nf1} = \frac{F_{11}^{cr}}{h_p w} = \tau_{nf} \frac{h_2}{h_p} \tag{51}$$

where h_p, as defined in (8), is the thickness of the equivalent element. The numerical index in the subscript of the failure stress notation is used to indicate the normal direction of the plane associated

DOI: 10.1002/nag

with this failure stress. For the general case of multiple categories, h_2 in (51) is replaced by the minimum thickness $h_{min} = \min\{h_1, h_2, \ldots, h_N\}$, where N is the total number of categories.

For the failure stress in the 2 direction, assume again that the original element is subjected to a stress resultant F_{22} as shown in Figure 3(a). Because $\varepsilon_{22}^{(1)} = \varepsilon_{22}^{(2)} = \delta_2/w$, both categories have the same normal stress in the 2 direction, that is, $\sigma_{22}^{(1)} = \sigma_{22}^{(2)} = E\delta_2/w$. This observation means that both categories will fail at the same time under tension in the 2 direction when their normal stress reaches the failure stress in tension of the material, that is, $\sigma_{22}^{(1)} = \sigma_{22}^{(2)} = \tau_{nf}$. Thus, the failure stress resultant is

$$F_{22}^{cr} = \tau_{nf}(h_1 l_1 + h_2 l_2). \tag{52}$$

The failure stress for pure tension of the equivalent element will be

$$\tau_{nf2} = \frac{F_{22}^{cr}}{h_p(l_1 + l_2)} = \tau_{nf}\frac{h_1 l_1 + h_2 l_2}{h_p(l_1 + l_2)}. \tag{53}$$

Using (8), we obtain

$$\tau_{nf2} = \tau_{nf}. \tag{54}$$

4.2.2. Failure stress for pure shear. Utilizing the same procedure we used to derive the failure stress for pure tension, we can easily obtain the results of failure stresses in pure shear as follows

$$\tau_{sf1} = \tau_{sf}\frac{h_2}{h_p}, \tag{55}$$

and

$$\tau_{sf2} = \tau_{sf}. \tag{56}$$

For a general case of multiple categories, h_2 in (55) is replaced by the minimum thickness h_{min} as in the case of tension.

4.2.3. Failure stress for pure compression. Similar to the cases of tension and shear, under pure compression in the 1 direction, failure will occur first in the thinnest category, which is assumed to be category 2 (i.e., $h_2 < h_1$) for the system in Figure 2(a). For compression, the direction of F_{11} should be reversed in the figure. If the force, F_{11}, is large enough, then we expect the thin ice in category 2 to be crushed and ridged. As ridging progresses, h_2 will increase until it reaches h_1, at which point the two categories are the same and become one. Further ridging will occur if F_{11} is large enough to also cause ice of thickness $h_1 = h_2$ to fail. If F_{11} is not large enough, then no further failure will occur. With this understanding of failure in compression, we make an assumption that failure initiates when category 2 begins to fail, then the same procedure as in the case of tension holds also for compression. The failure stresses in pure compression are

$$f_{c1}^{'} = f_c^{'}\frac{h_2}{h_p}, \tag{57}$$

and

$$f_{c2}^{'} = f_c^{'}. \tag{58}$$

As before, for multiple categories, h_2 in Equation (57) is replaced by the minimum thickness h_{min}.

DOI: 10.1002/nag

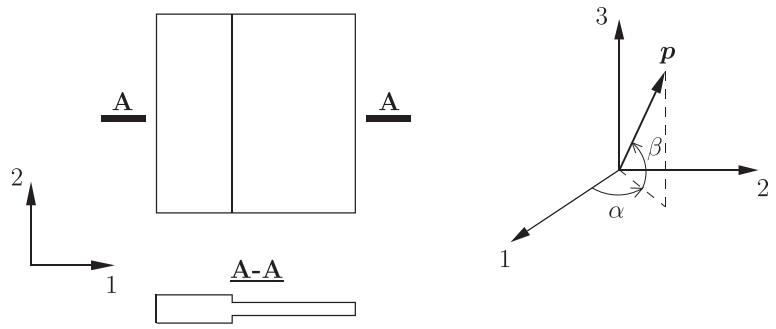

Figure 8. Direction of a unit vector $\boldsymbol{p}$ in the material coordinate system.

4.2.4. Failure stress in an arbitrary direction. The failure stress in the direction of a vector $\boldsymbol{p}$, defined in the material coordinate system as shown in Figure 8, is assumed to be interpolated from the basic values in the three material directions using a tensor projection operator as follows

$$\tau_p = (\tau_1 \boldsymbol{i} \otimes \boldsymbol{i} + \tau_2 \boldsymbol{j} \otimes \boldsymbol{j} + \tau_3 \boldsymbol{k} \otimes \boldsymbol{k}) \cdot (\boldsymbol{p} \otimes \boldsymbol{p}) \tag{59}$$

where $\{\tau_1, \tau_2, \tau_3\}$ are the failure stresses in the material directions 1, 2, and 3, respectively, and $\{\boldsymbol{i}, \boldsymbol{j}, \boldsymbol{k}\}$ are the unit vectors associated with these directions. Equation (59) applied to the failure stress in pure tension, shear, and compression reduces to the corresponding values for τ_i that we have derived in the previous sections. We remark that we assume equivalence between the 2 and 3 directions so failure stress in the 3 direction is the same as for the 2 direction. Let $\{\alpha, \beta\}$ denote the two spherical coordinates of $\boldsymbol{p}$ as shown in Figure 8, that is, $\boldsymbol{p} = (\cos\beta\cos\alpha)\boldsymbol{i} + (\cos\beta\sin\alpha)\boldsymbol{j} + (\sin\beta)\boldsymbol{k}$. Then, Equation (59) becomes

$$\tau_p = (\cos\beta\cos\alpha)^2\tau_1 + (\cos\beta\sin\alpha)^2\tau_2 + (\sin\beta)^2\tau_3. \tag{60}$$

4.3. Anisotropic failure curves

Having the values of failure stress in hand, we now can apply the formulation (47)–(49) for the anisotropic material of the equivalent element to determine the initial failure curve. Note that when we apply (47)–(49) to an anisotropic material, the values of $\{\tau_{nf}, \tau_{sf}, f_c^{'}\}$ depend on the direction of the crack plane following Equation (60). The first example for an anisotropic failure curve is shown in Figure 9(a). In this example, the original element has two categories as shown in Figure 9(b). The area of the two categories is the same, $l_1 = l_2$, but the thickness of the first category is three times larger than that of the second category, $h_1 = 3h_2$. The material employed in this example is material 1 in Table I. For this example, the material axes $\{1, 2, 3\}$ are taken to be coincident with the principal axes $\{\boldsymbol{p}_1, \boldsymbol{p}_2, \boldsymbol{p}_3\}$. In Figure 9(a), for comparison, we also plot the isotropic failure curve in which the material of the equivalent element is assumed to be isotropic. It can be seen that the anisotropic failure curve is smaller than the isotropic one because the failure stress under tension in the 1 direction of the anisotropic model is smaller than that of the isotropic model, that is, $\tau_{nf1} = (h_2/h_p)\tau_{nf} = 0.5\tau_{nf}$. This is obvious because the existence of thin ice in category 2 makes the 1 direction the weakest in tension.

Figure 10 illustrates the dependence of the failure curves on the thickness distribution. Consider again the case of two categories that have the same area fractions but different thicknesses. While the average thickness h_p is kept unchanged, the relative difference between h_1 and h_2 is varied as shown in the legend of Figure 10. Material 1 in Table I is used for this example, and the material axes are aligned with the principal axes as shown in Figure 9(b). It can be seen that the failure curves become smaller as the relative difference between h_1 and h_2 becomes larger. It is easier to break a mixture of ice as the ice in one category becomes thinner.

DOI: 10.1002/nag

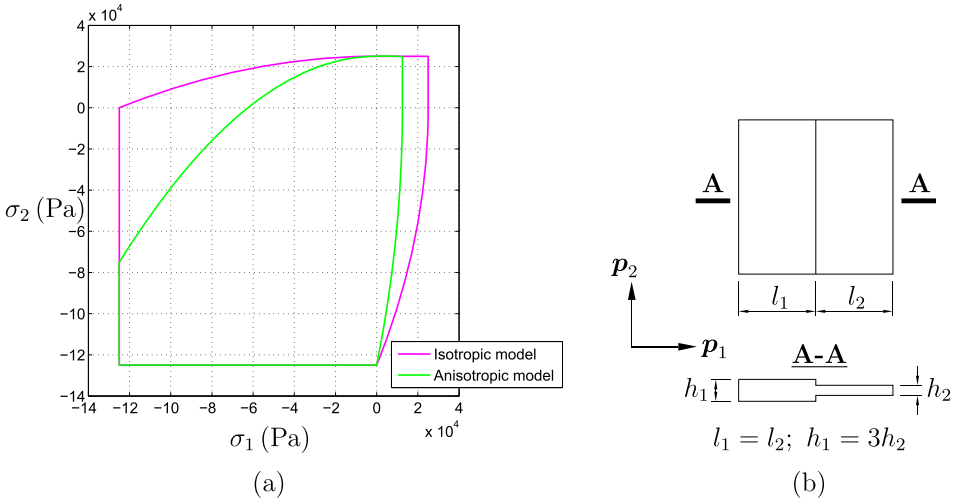

Figure 9. (a) Initial failure curves for the anisotropic model and the isotropic model for material 1 in Table I; (b) schematic of the thickness distribution of the original element used in this example.

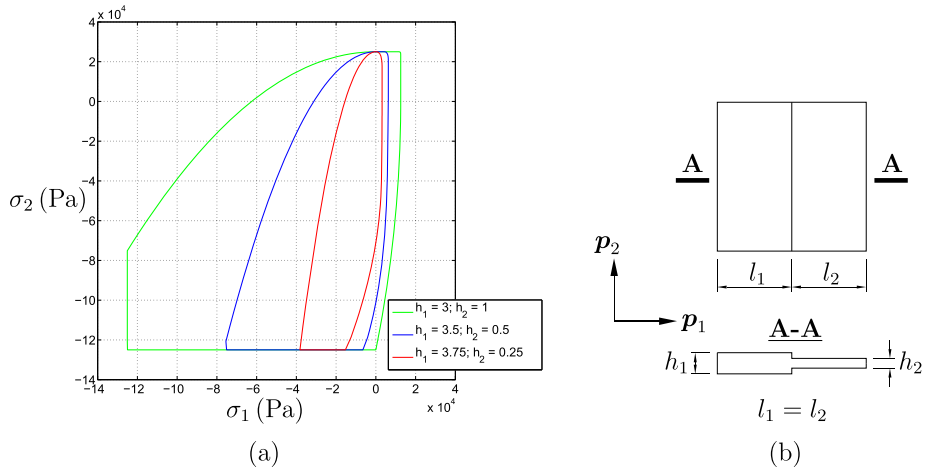

Figure 10. (a) Initial failure curves for the anisotropic model with different thickness distributions; (b) schematic of the thickness distribution of the original element used in this example.

5. EVOLUTION OF FAILURE

After failure has been initiated due to stress reaching the failure curve in stress space, it is assumed that in physical space, a discontinuity of displacement across the crack surface develops simultaneously with a reduction of the strength on this surface. A macrocrack is formed when the material completely loses its strength, and traction-free surfaces are created (provided that there is no external traction applied on the crack surfaces). In terms of $\boldsymbol{n}-\boldsymbol{s}$ components, the jump (i.e., displacement discontinuity) is denoted

$$[\boldsymbol{u}] = [u_n]\,\boldsymbol{n} + [u_s]\,\boldsymbol{s}. \tag{61}$$

The decohesion function (49) is modified to include a softening function, f_n, in order to include traction reduction in the model

$$F_n = \frac{\tau_s^2}{(s_m \tau_{sf})^2} + \exp\left(\kappa\left(\frac{\tau_n}{\tau_{nf}} + f_n\left(\frac{\langle -\sigma_{tt}\rangle^2}{f_c'^2} - 1\right)\right)\right) - 1. \tag{62}$$

DOI: 10.1002/nag

In order to specify the traction reduction, we introduce a material constant u_o as the value of the displacement discontinuity in the $\boldsymbol{n}$-direction when the macrocrack is formed. Then, we define the relation

$$f_n = \left\langle 1 - \frac{u_n}{u_o} \right\rangle. \tag{63}$$

With this definition, the softening function is non-negative and decreases linearly from 1 to 0 as the crack evolves from its initial failure state to a macrocrack. If there is no shear (i.e., $\tau_s = 0$), then when $f_n = 0$, it is only possible to have $F_n = 0$ if $\tau_n = 0$, that is, the traction on the failure surface is zero and the material has separated. With shear, it is possible to have a negative normal traction component on the failure surface. An associated flow rule is considered to compute the evolution of failure

$$[\dot{u}_n] = \dot{\omega} u_o \tau_{nf} \frac{\partial F_n}{\partial \tau_n} \qquad \text{and} \qquad [\dot{u}_s] = \dot{\omega} u_o \tau_{nf} \frac{\partial F_n}{\partial \tau_s} \tag{64}$$

where the superimposed dots denote derivatives with respect to time, and the common factor $u_o \tau_{nf}$ in these expressions is introduced to render the evolution parameter ω dimensionless.

The parameter u_o gives a length scale over which a macrocrack is formed. The failure energy is the energy required, per unit area of crack face, to open the crack. If a crack is opened in tension (mode I failure), then the failure energy is $0.5\tau_{nf} u_o$. This relation provides a means to determine the value of u_o.

To summarize the numerical algorithm, consider a square element of size w and thickness h_p as indicated in Figure 11(a). For an active crack with current components of discontinuity $[u_n]$ and $[u_s]$ assumed to be constant across the crack surface, assume further that the normal $\boldsymbol{n}$ to this crack has $\phi \neq \pm 90^o$ as indicated in Figure 11(b). (At the end of this section, we discuss the special case when $\phi = \pm 90^o$.) Denote $\bar{\boldsymbol{n}}$ and $\bar{\boldsymbol{t}}$ unit vectors in the $1-2$ plane that are perpendicular and tangent to the intersection of the crack plane and the $1-2$ plane. Note that $\bar{\boldsymbol{n}}$ is along the projection of $\boldsymbol{n}$ onto the $1-2$ plane. Then, the discontinuity in the $\bar{\boldsymbol{n}}$ and $\bar{\boldsymbol{t}}$ directions are

$$[u_{\bar{n}}] = [\boldsymbol{u}] \,.\, \bar{\boldsymbol{n}} \qquad \text{and} \qquad [u_{\bar{t}}] = [\boldsymbol{u}] \,.\, \bar{\boldsymbol{t}} \tag{65}$$

where $[\boldsymbol{u}]$ is defined in (61). The smeared crack approach (e.g., [10, 30]) is used to compute the decohesive strains in $\bar{\boldsymbol{n}}-\bar{\boldsymbol{t}}$ as

$$\begin{aligned} \varepsilon^{dc}_{\bar{n}\bar{n}} &= \frac{[u_{\bar{n}}]}{w_n} \\ \varepsilon^{dc}_{\bar{n}\bar{t}} &= \frac{[u_{\bar{n}}]}{2w_n} \\ \varepsilon^{dc}_{\bar{t}\bar{t}} &= 0 \end{aligned} \tag{66}$$

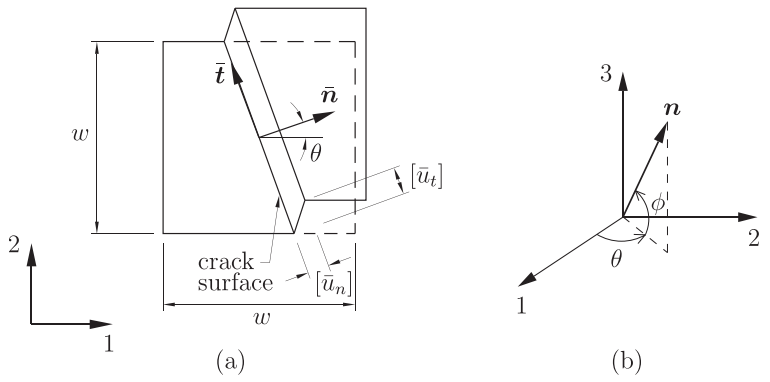

Figure 11. (a) Sketch of the relationship between the displacement discontinuity and decohesive strains; (b) normal vector to the crack surface in the global coordinate system.

DOI: 10.1002/nag

where w_n is the crack length, $w_n = w/\cos\theta$ in Figure 11. The stress rate is then computed as

$$\begin{aligned}\dot{\sigma}_{11} &= C_{11}\left(\dot{\varepsilon}_{11} - \dot{\varepsilon}_{11}^{dc}\right) + C_{12}\left(\dot{\varepsilon}_{22} - \dot{\varepsilon}_{22}^{dc}\right)\\ \dot{\sigma}_{22} &= C_{12}\left(\dot{\varepsilon}_{11} - \dot{\varepsilon}_{11}^{dc}\right) + C_{22}\left(\dot{\varepsilon}_{22} - \dot{\varepsilon}_{22}^{dc}\right)\\ \dot{\tau}_{12} &= C_{33}\left(\dot{\varepsilon}_{12} - \dot{\varepsilon}_{12}^{dc}\right)\end{aligned} \tag{67}$$

where $\{C_{11}, C_{12}, C_{22}, C_{33}\}$ are the components of the stiffness matrix, which is the inverse of the compliance matrix defined in (40), but rotated to the global coordinate system, $\dot{\varepsilon}_{ij}$ $(i, j \in \{1, 2\})$ is the strain rate, and $\dot{\varepsilon}_{ij}^{dc}$ $(i, j \in \{1, 2\})$ is the decohesive strain obtained by transforming the components given in (66) to the global coordinate system.

For the special case when the failure surface is in the 1−2 plane (i.e., $\phi = \pm 90^o$), the material fails when both principal stresses σ_1 and σ_2 are negative. These failure modes, as illustrated in Figure 7, make the thickness increase. This mode of failure is analogous to buckling of a column under compression. After one of the principal stresses in the thinnest ice reaches the critical value of $f_c^{'}$, and the loading continues to provide compression of the material, the thickness starts increasing while the principal stress in the thin ice maintains the value of $f_c^{'}$. The result for the effective compressive strength is that it increases according to (57) as the ice thickens. The increment of thickness is computed from volume conservation of the basic element.

6. NUMERICAL EXAMPLES

In this section, we present some numerical examples to illustrate features of the developed model. The material-point method (MPM) [26, 31] is employed to solve the momentum equation. Examples involving tensile and shear failure are considered to illustrate the typical features of the developed model. In our numerical implementation of the elastic-decohesive constitutive model, we represent a lead predicted by the model with a line through the center of an element in the discretization, and the line traverses the element. The width of the predicted lead is determined by the jump in displacement computed during the evolution of failure. We do not attempt to connect the leads from one element to the next. Any alignment that occurs is solely due to the stress state in the ice that makes a particular lead orientation favorable. This representation of leads is perhaps the simplest possible, and the performance of the numerical algorithm based on these simplifying assumptions, as compared with more complicated approaches, warrants further, future investigation.

As noted in the last section, displacement discontinuities obtained from the decohesive model are used to obtain smeared crack-strain components. The crack strains produce a stress-softening feature within the element. If the element is larger than a critical size, there is a stress reversal, which cannot be handled without a major (unknown) modification to the numerical procedure. If square elements of side Δx are used, stress reversal does not occur provided Δx is less than a critical length, $\Delta x_{cr} \approx u_o E/\tau_{nf}$. Typically, an element size somewhat smaller than the critical size is used to preclude reversal for all paths. In the examples, we use an artificially large value of u_o to avoid stress reversals.

6.1. Example 1: a region of ice under uniaxial tensile stress

The first example shows the effect of the thickness distribution on the formation of cracks in a pure opening mode. Consider a region of ice with length $L = 70\,\text{km}$ and width $W = 30\,\text{km}$ as shown schematically in Figure 12. The left and right sides of the region have a prescribed horizontal velocity of zero and v_o, respectively, and a prescribed vertical traction of zero (i.e., they are free to move vertically). The value of v_o is chosen to be small enough so that the numerical dynamic solution approximates the static solution. For this example, the value of v_o is 0.001 m/s. A material with properties shown in Table III is employed for this example. The region has a uniform thickness $h = 2\,\text{m}$ except in a narrow sub-region toward the left side that has a thickness distribution with two categories as shown in the Figure 12. Thickness and area fraction of the categories are taken to be

DOI: 10.1002/nag

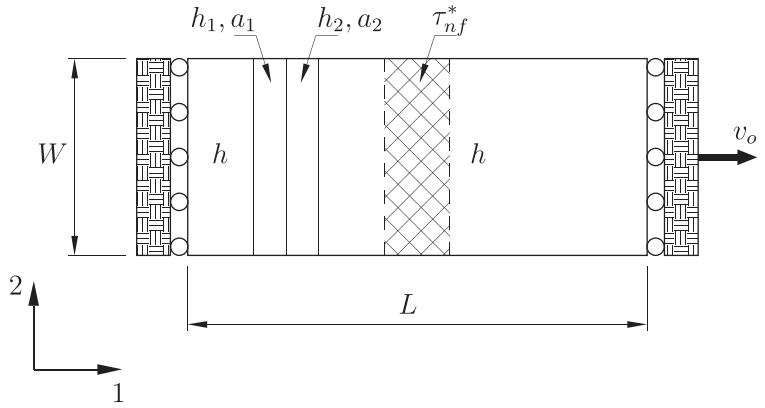

Figure 12. Schematic of a region of ice under a horizontal stretch.

Table III. Properties of the material employed for the problem shown in Figure 12.

Young's modulus (kPa)	Poisson's ratio	τ_{nf} (kPa)	τ_{sf} (kPa)	$f_c^{'}$ (kPa)	s_m	u_o (m)
1000	0.36	25	75	125	4	3000

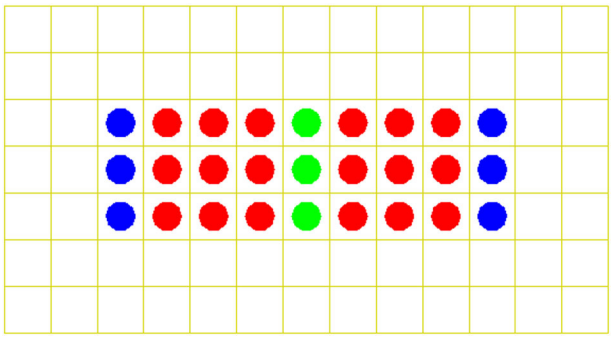

Figure 13. Background grid and different types of material points used in the numerical simulation of the problem in Figure 12. Blue circles represent rigid material points, the red circles are material points having τ_{nf}, and the green circles are material points having τ_{nf}^*.

$h_1 = 1\,\text{m}$ and $h_2 = 3\,\text{m}$, and $a_1 = a_2 = 0.5$. This set up is equivalent to a thickness distribution of $g = \delta(h-2)$ except in the narrow strip where $g = 0.5\delta(h-1) + 0.5\delta(h-3)$. Note that the average thickness associated with these thickness distributions is $h_p = 2\,\text{m}$, everywhere. Also in the center of the region, the material is chosen to be slightly weaker than the rest with a smaller value of failure stress in pure tension $\tau_{nf}^* = 0.9\tau_{nf}$ as shown in Figure 12.

For numerical simulation using the MPM, the region is initially discretized into 7×3 cells on the background grid of 13×7 cells as shown in Figure 13. The cell size is 10 km on each side, and there is one material point per cell initially. To model boundaries whose velocities are prescribed, additional regions made of a rigid material (i.e., material having an infinite mass) are employed. These rigid regions have a velocity equal to the prescribed value. In Figure 13, the blue circles are rigid material points, the red circles are material points having τ_{nf}, and the green circles are material points having τ_{nf}^*. The material points carry physical information of the problem and move in a Lagrangian manner. Details about the MPM can be found in the aforementioned references.

The simulation is from an initial, undeformed state until a complete vertical crack is formed through the region. Figure 14 shows the numerical results of the normalized crack opening, u/u_o, where u is the crack opening, at the end of the simulation time. To illustrate the features of the

DOI: 10.1002/nag

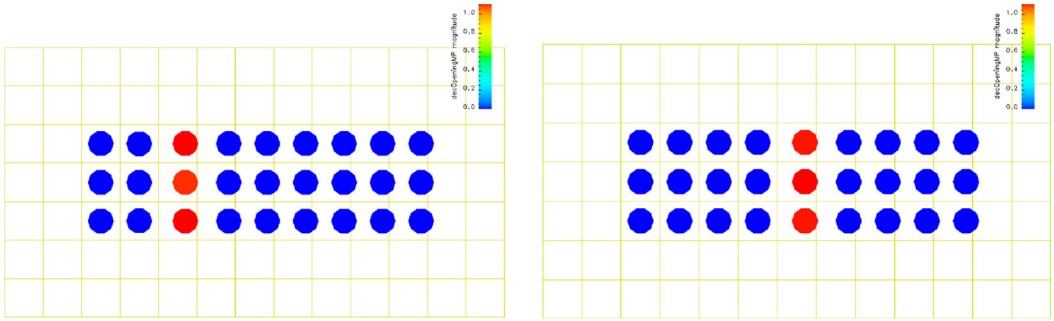

Figure 14. Normalized crack opening: (a) using present anisotropic model and (b) using the model developed by Schreyer *et al.*, [10].

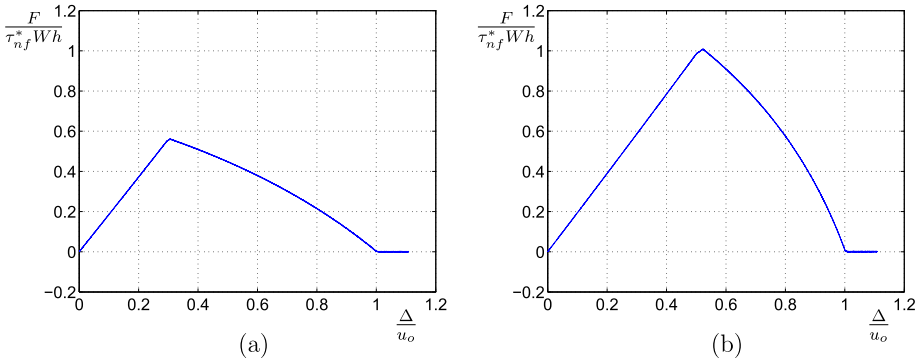

Figure 15. Normalized resultant force versus displacement of the right end for the specimens shown in Figure 14: (a) using the present anisotropic model and (b) using the model developed by Schreyer *et al.*, [10].

current model, the results are obtained using the anisotropic constitutive model (Figure 14(a)) and the original constitutive model developed by Schreyer *et al.*, [10] (Figure 14(b)). It can be seen that, for the original model, the crack occurs in the region associated with the material having τ_{nf}^*, while the anisotropic model shows the crack occurring in the region where there is a thickness distribution with thin ice. This fact illustrates the desired feature of the anisotropic model that it is able to predict preferentially failure in a region containing thin ice while the original model is not. Figure 15 shows the normalized horizontal force versus displacement at the right end of the region. The force increases linearly up to a maximum value at which the initial failure occurs, followed by a softening stage in which the force reduces to zero during the evolution from a micro crack (i.e., initial failure) to a macrocrack (i.e., a complete crack where the material is completely separated to create traction-free surfaces). The complete crack is formed when the total crack opening is equal to u_o. It can be seen that, in the original model, the initial failure occurs when the stress component σ_{11} reaches the critical value τ_{nf}^*, while in the anisotropic model, the initial failure occurs when σ_{11} is still far below the critical value τ_{nf}^*. This behavior occurs because of the dependence of the failure stress on the minimum thickness in the thickness distribution as shown in Equation (51). The displacements at the end of the softening stage of the two models are the same and equal to u_o. However, the fracture energy (which is the area under the force-displacement curve) of the anisotropic model is half that of the original model. In other words, in the anisotropic model, less energy is needed to break the region due to the existence of thin ice in the region. This feature cannot be represented in the original model. Moreover, the slope of the linear elastic loading stage is different in the two models due to the modified effective elastic moduli resulting from the thickness induced anisotropy derived in Section 3.

DOI: 10.1002/nag

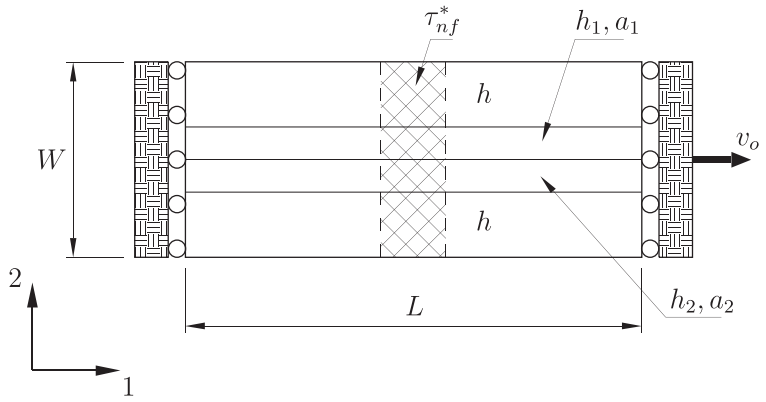

Figure 16. Schematic of a region of ice under a horizontal stretch.

Now, we want to show the effect of the orientation of the thickness distribution to the loading by changing the configuration of thin ice. The vertical sub-region with thin ice in Figure 12 now becomes a horizontal sub-region as shown in Figure 16. As before, we set $h = 2\,\text{m}$, $h_1 = 0.5\,\text{m}$, $h_2 = 1.5\,\text{m}$, and $a_1 = a_2 = 0.5$. Using the same discretization as before, shown in Figure 13, we obtain the results for crack opening and the relation between the force and displacement at the right end of the region. The results are the same for both constitutive relations and also the same as that of example 1 using the original model as shown in Figures 14(b) and 15(b). There is no difference between the new anisotropic model and the original model with this orientation of the thickness distribution. The extensional modulus and failure stress in the 1 direction of the anisotropic material (i.e., the material containing the two-category thickness distribution) are the same as those of the isotropic material (i.e., the material of the region with uniform thickness) as shown in Equations (24) and (54).

6.2. Example 2: a region of ice under shear loading

This example is chosen to illustrate the effect of a thickness distribution on the formation of cracks in a shearing mode. Consider a square region of ice with size $L = 100\,\text{km}$, as shown schematically in Figure 17(a). The left side of the region has zero velocity prescribed. A wind field is uniformly applied to the region in the vertical direction, and the wind velocity is taken to be a linear function of time (i.e., $v_1^{wind} = 0$ and $v_2^{wind} = A_o t$ where the value of constant A_o is 10^{-6} and t is time). Similar to example 1, there is a thin sub-region that is composed of a thickness distribution containing two categories whose thicknesses and area fractions are (h_1, a_1) and (h_2, a_2), respectively. The remainder of the region has uniform thickness $h = 2\,\text{m}$. Numerical values are chosen as before to be $h_1 = 1\,\text{m}$, $h_2 = 3\,\text{m}$, and $a_1 = a_2 = 0.5$. For the numerical simulation using the MPM, the region is initially discretized into 10×10 cells on the background grid of 14×14 cells as shown in Figure 17(b). All cells are 10 km on a side, and there is one material point per cell initially. Additional material points are used to model the prescribed velocity boundary condition of the left side of the region. Figure 17(b) also shows different types of material points used in the simulation: the blue ones are material points whose velocities are prescribed, the red ones are material points having uniform thickness $h = 2\,\text{m}$, and the green ones are material points having the aforementioned thickness distribution with two categories. The material whose properties are shown in Table IV is employed for this example. Note that for this material, the failure stress in shear is smaller than the nominal tensile failure stress, rather than three times the tensile failure stress as used in the previous example. These values are chosen to explicitly illustrate mixed-mode rather than tensile-mode failure.

The simulation runs from the initial, undeformed state until a complete crack propagates across the region. Again, to illustrate the features of the current model, the simulation is compared with the original model developed by Schreyer *et al.*, [10]. Figure 18 shows the normalized crack opening u/u_o at time $t = 203040\,\text{s}$ generated by the two models. It can be seen that with the current model

DOI: 10.1002/nag

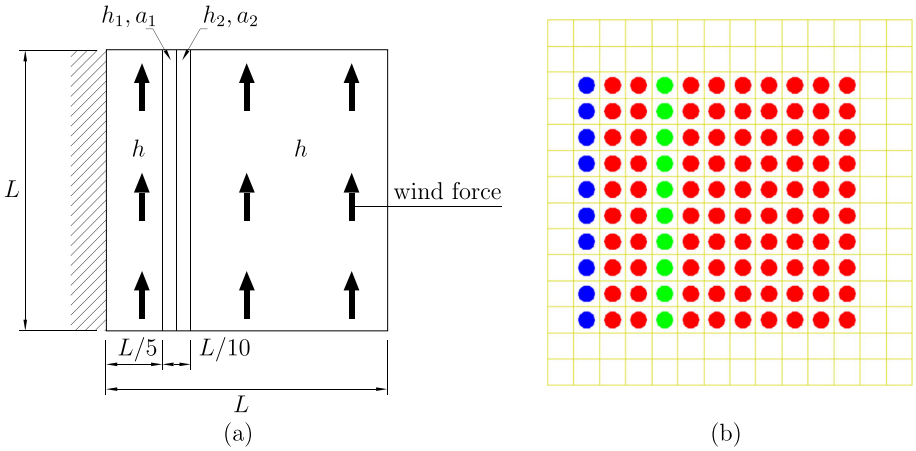

Figure 17. (a) Schematic of a region of ice under wind loading producing shear; (b) background grid and location of the different types of material points used in the numerical simulation.

Table IV. Properties of the material employed for the problem shown in Figure 17.

Young's modulus (kPa)	Poisson's ratio	τ_{nf} (kPa)	τ_{sf} (kPa)	$f_c^{'}$ (kPa)	s_m	u_o (m)
1000	0.36	25	15	125	4	3000

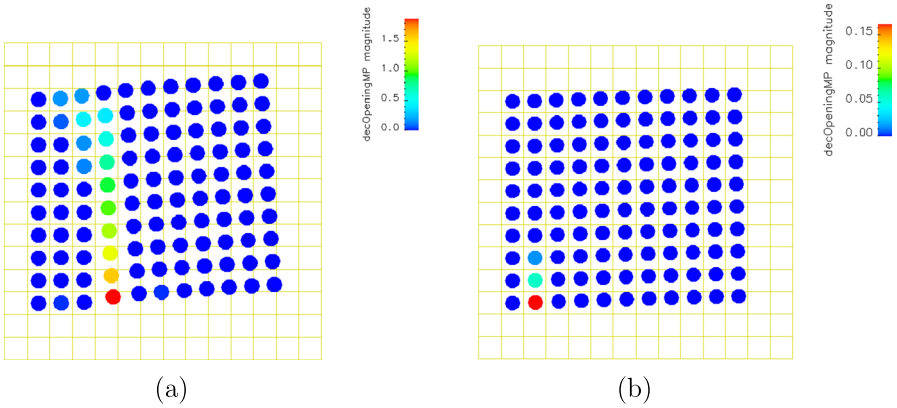

Figure 18. Normalized crack opening at a certain time: (a) using the present anisotropic model and (b) using the original model developed by Schreyer *et al.*, [10].

as shown in Figure 18(a), the crack due to shear occurs in the area where thin ice exists (i.e., the area with the two-category thickness distribution). However, this is not the case for the original model, as can be seen in Figure 18(b), in which the crack due to shear occurs in the area of high shear stress regardless of the existence of thin ice. In this example, the average thickness that is the property used in the original model is constant over the whole region.

7. CONCLUSIONS

In a two-dimensional model of the Arctic ice cover, ice of varying thickness has varying stiffness and strength. In global climate models, ice thickness is tracked through a thickness distribution function that evolves with the flowing ice due to mechanical redistribution and due to thermodynamic processes. In this paper, we use the thickness distribution to develop an effective or equivalent material

DOI: 10.1002/nag

description for an element of ice with varying thickness. The result is a constant thickness equivalent element with an anisotropic, elastic response. Specifically, the equivalent material is orthotropic with material axes aligned normal and tangential to a lead direction. This model more accurately accounts for the deformation of pack ice because the character of internal ice stress depends strongly on the existence of thin ice. In particular, the model can represent implicitly the existence of open water in the thickness distribution because the effective moduli go to zero as open water appears in the thickness distribution. It should be noted that the developed internal stress in the ice also depends on the orientation of the external forcing relative to the orientation of a lead, a feature also captured by the model.

In the failure regime, a decohesive constitutive model determines the lead orientation as well as the amount of lead opening and any subsequent closing. A decohesion function, which is a function of traction on a potential crack surface and of the material strengths in failure, is employed to predict the initial failure of the material. In contrast to the original decohesive model developed in [10], the material strengths depend on the direction of the crack surface. The strengths in the directions of the material basis vectors are determined with reference to the thickness distribution within the element of ice. The strength in any direction is interpolated from the basic strengths in the three material directions. In both the elastic and failure regimes, we assume that the thickness distribution is oriented with any existing lead and also associate the thinnest part of the thickness distribution with the lead. This assumption precludes the necessity for two distributions, one associated with and oriented with the lead ice and the other associated with intact ice.

Typical examples for initial failure curves are presented to illustrate the capability of the model to predict the failure behavior of the ice with a thickness distribution. Evolution of failure is also discussed where an associated flow rule is proposed to determine the discontinuity formation across the crack surface. The developed constitutive relation is compatible with any domain-based numerical method such as the finite element method or the MPM. We use the MPM to model regions of ice under idealized loading, with idealized thickness distributions. The examples are chosen to illustrate the change in ice behavior when the orientation of loading changes with respect to the orientation of a lead. The model predicts our intuitive notion that tensile failure should occur in thin, lead ice if tension exists across a lead. However, the thin lead ice does not impact failure if the tension exists along the lead direction. Another example shows how shear failure can also occur preferentially in thin lead ice.

This work demonstrates a model that explicitly accounts for leads through an elastic-decohesive constitutive model for sea ice. Moreover, the rheology is tightly connected to the thickness distribution so that the mechanics reflects essential properties of sea ice. Specifically, sea ice is heterogeneous and anisotropic in behavior in the aggregate because of the presence of leads, ridges, and other flaws. Future work will assess this formulation in the context of a global climate model where its performance can be analyzed in the presence of naturally occurring and complicated forcing. In such a setting, simplifying assumptions related to the thickness distribution in leads and the piecewise representation of leads can be better evaluated.

ACKNOWLEDGEMENT

This work was partially supported by the National Science Foundation under grant ARC-1023667 to the University of New Mexico.

REFERENCES

1. Thorndike AS, Rothrock DA, Maykut GA, Colony R. The thickness distribution of sea ice. *Journal of Geophysical Research* 1975; **80**:4501–4513.
2. Thorndike AS, Maykut GA. On the thickness distribution of sea ice. *AIDJEX Bulletin* 1973; **21**:31–48.
3. Timco GW, Weeks WF. A review of the engineering properties of sea ice. *Cold Regions Science and Technology* 2010; **60**:107–129.
4. Coon MD, Maykut GA, Pritchard RS, Rothrock DA, Thorndike AS. Modeling the pack sea ice a an elastic-plastic material. *AIDJEX Bull* 1974; **24**:1–105.
5. Hibler WD. A dynamic thermodynamic se ice model. *Journal of Physical Oceanography* 1979; **9**:815–845.

DOI: 10.1002/nag

6. Hibler WD, Schulson EM. On modeling sea ice fracture and flow in numerical investigation of climate. *Annals of Glaciology* 1997; **25**:26–32.
7. Hibler WD. Sea ice fracturing on the larger scale. *Engineering Fracture Mechanics* 2001; **68**:2013–2043.
8. Hunke EC, Dukowicz K. An elastic-viscous-plastic model for sea ice dynamics. *Journal of Physical Oceanography* 1997; **27**:1849–1867.
9. Hunke EC. Viscous-plastic sea ice dynamics with the EVP model: linearization issues. *Journal of Computational Physics* 2001; **170**:18–38.
10. Schreyer HL, Sulsky DL, Munday LB, Coon MD, Kwok R. Elastic-decohesive constitutive model for sea ice. *Journal of Geophysical Research* 2006; **111**:1–21.
11. Sulsky D, Peterson K. Toward a new elastic-decohesive model of Arctic sea ice. *Physica D* 2011; **240**:1674–1683.
12. Hibler WD, Schulson EM. On modeling the anisotropic failure and flow of flawed sea ice. *Journal of Geophysical Research* 2000; **105**:17105–17120.
13. Wilchinsky AV, Feltham DL. A continuum anisotropic model of sea-ice dynamics. *Proceedings of the Royal Society of London Series A* 2004; **460**:2105–2140.
14. Wilchinsky AV, Feltham DL. Anisotropic model for granulated sea ice dynamics. *Journal of the Mechanics and Physics of Solids* 2006; **54**:1147–1185.
15. Tsamados M, Feltham DL, Wilchinsky AV. Impact of a new anisotropic rheology on simulations of Arctic sea ice. *Journal of Geophysical Research-Oceans* 2013; **118**:91–107.
16. Wilchinsky AV, Feltham DL. Modeling the rheology of sea ice as a collection of diamond-shaped floes. *Journal of Non-Newtonian Fluid Mechanics* 2006; **138**:22–32.
17. Girard L, Bouillon S, Weiss J, Amitrano D, Fichefet T, Legat V. A new modeling framework for sea-ice mechanics based on elasto-brittle rheology. *Annals of Glaciology 52(57) 2011* 2011; **52**:123–132.
18. Coon MD, Knoke GS, Echert DC. The architecture of an anisotropic elastic-plastic sea ice mechanics constitutive law. *Journal of Geophysical Research* 1998; **103**:21,915–21,929.
19. Bitz CM, Lipscomb WH. An energy-conserving thermodynamic model of sea ice. *Journal of Geophysical Research* 1999; **104**(C7):15669–15677.
20. Lipscomb WH, Hunke EC. Modeling sea ice transport using incremental remapping. *Monthly Weather Review* 2004; **132**:1341–1354.
21. Lipscomb WH, Hunke EC, Maslowski W, Jakacki J. Ridging, strength, and stability in high-resolution sea ice models. *Journal of Geophysical Research* 2007; **112**:C03S91.
22. Daniel IM, Ishai O. *Engineering Mechanics of Composite Materials*. Oxford University Press: New York, 1994.
23. Hyer MW. *Stress Analysis of Fiber-Reinforced Composite Materials*. McGraw-Hill: New York, 1998.
24. Gray JMNT, Morland LW. A two-dimensional model for the dynamics of sea ice. *Philosophical Transactions of the Royal Society of London, Series A* 1994; **347**:219–290.
25. Rothrock DA. The energetics of the plastic deformation of pack ice by ridging. *Journal of Geophysical Research* 1975; **80**(33):4514–4519. DOI: 10.1029/JC080i033p04514.
26. Sulsky D, Schreyer H, Peterson K, Kwok R, Coon M. Using the material-point method to model sea ice dynamics. *Journal of Geophysical Research* 2007; **112, C02S90**.
27. Wilchinsky AV, Feltham DL. Rheology of Discrete Failure Regimes of Anisotropic Sea Ice. *Journal of Physical Oceanograph* 2012; **42**:1065–1082. DOI: 10.1175/JPO-D-11-1078.1.
28. Lipscomb WH. Remapping the thickness distribution in the sea ice models. *Journal of Geophysical Research* 2001; **106**:13989–14000.
29. Schulson EM. Brittle failure of ice. *Engineering Fracture Mechanics* 2001; **68**:1839–1887.
30. Rashid YR. Analysis of prestressed concrete pressure vessels. *Nuclear Engineering and Design* 1968; **7**:334–355.
31. Sulsky D, Zhou S-J, Schreyer HL. Application of a particle-in-cell method to solid mechanics. *Computer Physics Communications* 1995; **87**:236–252.

DOI: 10.1002/nag